Ceramics International 50 (2024) 2259–2270

Contents lists available at ScienceDirect

Ceramics International

journal homepage: www.elsevier.com/locate/ceramint

Surface integrity study of ZrO_2 ceramic for ultrasonic vibration-assisted polishing processing

Chao Zhang, Fanwei Meng, Yingdong Liang, Tianbiao Yu *

School of Mechanical Engineering and Automation, Northeastern University, Shenyang, 110819, China

ARTICLE INFO

Handling Editor: Dr P. Vincenzini

Keywords:
Surface integrity
ZrO_2 ceramic
Hard and brittle materials
UVAP processing

ABSTRACT

Due to the unique physical property, the surface integrity is a critical indicator to characterize the processing quality for hard and brittle materials. In this study, the ZrO_2 ceramic is taken as a representative to investigate the surface integrity during ultrasonic vibration-assisted polishing (UVAP) processing. The effects of processing parameters on surface micro-morphology, surface hardness, scratch property and residual stress are analyzed by UVAP orthogonal experiments. The experiment results indicate that the UVAP processing can effectively improve the surface integrity of the ZrO_2 ceramic. The research results are of great significance in guiding the UVAP controlled processing of hard and brittle materials.

1. Introduction

The ZrO_2 ceramic has excellent biocompatibility and mechanical property. For biomedicine, the ZrO_2 ceramic has great application prospects in the field of oral and orthopedic restoration. First of all, the ZrO_2 ceramic has a low probability of rejection with the human body. In appearance, the surface color of ZrO_2 ceramic is similar to that of human teeth. These characteristics are not fully available for conventional titanium implant materials. Currently, many scholars are exploring the preparation of composite materials containing ZrO_2 ceramic and other biomaterials. In the future, there will be more human hard tissue substitutes such as bones or joints made from ZrO_2 ceramic matrix composites for human life [1–3]. After entering the 21st century, the ZrO_2 ceramic has been used as functional and structural materials on a large scale. In the field of mechanical engineering, the ZrO_2 ceramic is gradually replacing some wear-prone or high-temperature-resistant devices, such as cylinder liners, valves, and bearings, due to the excellent wear-resistant properties. The ZrO_2 ceramic possesses optoelectronic properties that make it also irreplaceable in the field of electronic communications. The performance of electronic communication components such as fiber optic connectors and sensors made from the ZrO_2 ceramic is greatly improved compared to metal or polymer materials [4–6].

Generally, there has been a dramatic increase in demand for part surfaces with nanoscale surface finishes and higher dimensional accuracy in recent years. Due to the limitations of the traditional polishing processing, many scholars seek new polishing methods to improve the machining efficiency and surface quality, such as jet polishing, electrorheological polishing, and so on [7–9]. As one of the new processing methods developed in recent years, UVAP technology is not only capable of processing traditional plastic materials, but also performs well in the processing of hard and brittle materials as well as difficult-to-machine materials with complex curved shapes [10,11]. In terms of surface quality, UVAP technology for wafer edges was investigated by Kobayashi et al. [12]. From the results, the wafer speed v and polishing pressure P had a greater influence on the wafer edge roughness. The improvement of wafer edge surface quality by UVAP was 31.7 % compared to the result without applying ultrasonic vibration. Suzuki [13,14] et al. conducted experiments on tiny aspherical lens molds using the UVAP technique. In this case, the ultrasonic amplitude was 10 μm, the frequency was 25 kHz, and the mold material was WC. Finally, a surface with roughness of 7 nm and face shape accuracy of 70 nm was obtained. In addition, Suzuki et al. further proposed to process the tiny aspherical lens molds by two-dimensional UVAP technique. The longitudinal and bending vibration frequencies were 28.9 kHz and 22.4 kHz, respectively. The longitudinal and bending vibration amplitudes were 40 μm and 30 μm, respectively. The final roughness Rz of the mold surface was reduced to 8 nm. Sun [15] and Wu et al. [16] conducted UVAP experiments on micro-structured sections of brittle materials such as SiC, and found that ultrasonic vibration was the primary reason affecting the material removal rate and surface quality. The experimental results showed that UVAP can efficiently remove the sub-surface

* Corresponding author.
E-mail address: tianbiaoyudyx@gmail.com (T. Yu).

https://doi.org/10.1016/j.ceramint.2023.10.344
Received 18 September 2023; Received in revised form 22 October 2023; Accepted 30 October 2023
Available online 31 October 2023

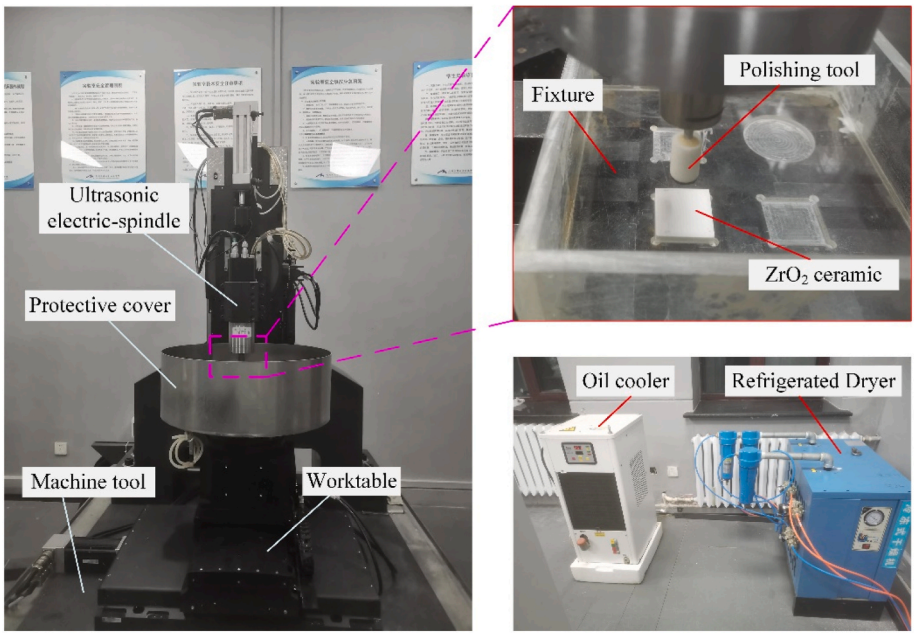

Fig. 1. The UVAP machine tool.

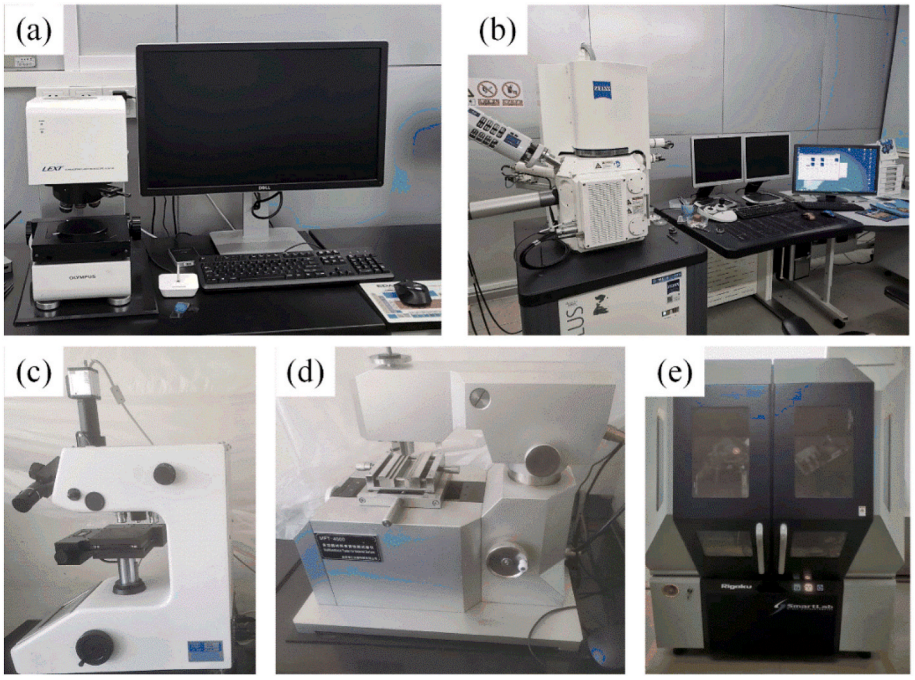

Fig. 2. The measuring instruments, (a) 3D laser confocal microscope, (b) scanning electron microscope, (c) hardness tester, (d) multifunctional tester for material surface, (e) polycrystalline XRD diffractometer.

Table 1
The processing parameters during UVAP.

Parameters	Value
Processing time/s	1800
Feed rate/ mm • s^{-1}	1
Diameter of polishing tool/mm	10
Pre-polishing force/N	8
Size of workpiece/mm	20 × 20 × 5

cracks from microstructures. In addition, UVAP can improve the face shape accuracy while improving the polishing efficiency.

Fan et al. [17] proposed a UVAP material removal exponential model. The model not only considered the processing parameters, but also included the influence of the dimensional nature of abrasive particles, the topology parameters of the polishing tool and the material property of the polishing slurry. The material removal profile after UVAP was obtained by numerical integration. Considering the effect of abrasive particles on the profile depth, Wang et al. [18] modeled the linear removal intensity of cutting abrasive particles and derived the material removal depth function by integrating along the contact path of

Table 2
The orthogonal experiments design during UVAP.

No.	Spindle speed	Ultrasonic amplitude	Particle size	No.	Spindle speed	Ultrasonic amplitude	Particle size
1#	2000 rpm	0 μm	0.05 μm	6#	5000 rpm	8 μm	0.05 μm
2#	2000 rpm	4 μm	0.5 μm	7#	8000 rpm	0 μm	1 μm
3#	2000 rpm	8 μm	1 μm	8#	8000 rpm	4 μm	0.05 μm
4#	5000 rpm	0 μm	0.5 μm	9#	8000 rpm	8 μm	0.5 μm
5#	5000 rpm	4 μm	1 μm				

Table 3
The material properties of the ZrO_2, polyurethane and diamond.

Materials	Densities (g/cm^3)	Young's modulus (GPa)	Poisson's ratio	Vickers hardness (GPa)
ZrO_2	5.85	205	0.22	1200
Diamond	3.52	1000	0.07	50
Polyurethane	0.49	2.29×10^{-3}	0.47	–

the polishing tool. Li [19] and Shi et al. [20] investigated the surface quality and material removal process in UVAP from the perspective of SPH-coupled FEM. The abrasive particles were categorized into three mechanical states: two-body wear, three-body wear, and free-state. The abrasive particles of two-body wear cut the workpiece with horizontal-normal sinusoidal vibration, while the abrasive particles of free-state and three-body wear impact the workpiece. Wang et al. [21] simulated the UVAP processing of single-crystal silicon from the molecular dynamics point of view. The response process by an individual abrasive particle scratching the workpiece at the nanoscale was established. The material removal, phase transition, stress, potential energy, and cutting force were analyzed. Sheng et al. [22] investigated the UVAP processing of sapphire using the molecular dynamics approach. The effects of abrasive particle size, polishing speed, ultrasonic amplitude, and frequency on the polishing effect were explored in terms of temperature, average friction coefficient, stress distribution, subsurface damage, number of atoms removed, surface morphology and polishing force.

In summary, most of the previous studies have been conducted on the material removal characteristics of UVAP processing. Many scholars have made a lot of efforts on the material removal mechanism, processing efficiency and processing accuracy of the UVAP technique. The surface integrity studies for ceramic materials during UVAP processing are rare. In this study, the surface micro-morphology, surface roughness, surface hardness, scratching property and residual stress of the ZrO_2 ceramic are investigated during UVAP processing. Theoretically, this study is valuable for improving the surface integrity of the ZrO_2 ceramic during UVAP processing. The study is of great significance in guiding the UVAP controlled processing of hard and brittle materials.

2. Experimental methods and design

Surface integrity experiments for the ZrO_2 ceramic are performed on the UVAP machine tool. Fig. 1 is the UVAP machine tool. The ultrasonic generator produces a high-frequency vibration signal that is transmitted to the ultrasonic spindle. The ultrasonic spindle drives the polishing tool to produce axial ultrasonic vibration through the built-in amplitude-change rod. The oil cooler realizes ultrasonic spindle cooling by the principle of refrigerant evaporation and heat absorption. All operations of the machine tool are performed on the control cabinet, which receives the motion commands from the software and controls the spindle and table motion of the machine tool.

The workpiece is fixed at the acrylic fixture during the UVAP processing. The scratching property and surface hardness are measured by the multifunctional tester for material surface (MFT-4000) and hardness tester (MH-500), respectively. In the measurement of scratching property, the scratching path is approximately perpendicular to the polishing path. The loading time is 2min, the upper limit of the loading force is set to 50 N, and the scratching length is 10 mm. For the simplicity of analysis, the scratching coefficients of the loading force between 30 N and 40 N are uniformly studied. For the measurement of hardness, three equally spaced measuring points are selected on the workpiece surface and consider the average value as the surface hardness. The loading force is 1000 N and the distance between the measuring points is 400 μm.

The polycrystalline XRD diffractometer (D8ADVANCE) and scanning electron microscope (SEM, FEI QUANTA 600) are used to measure the

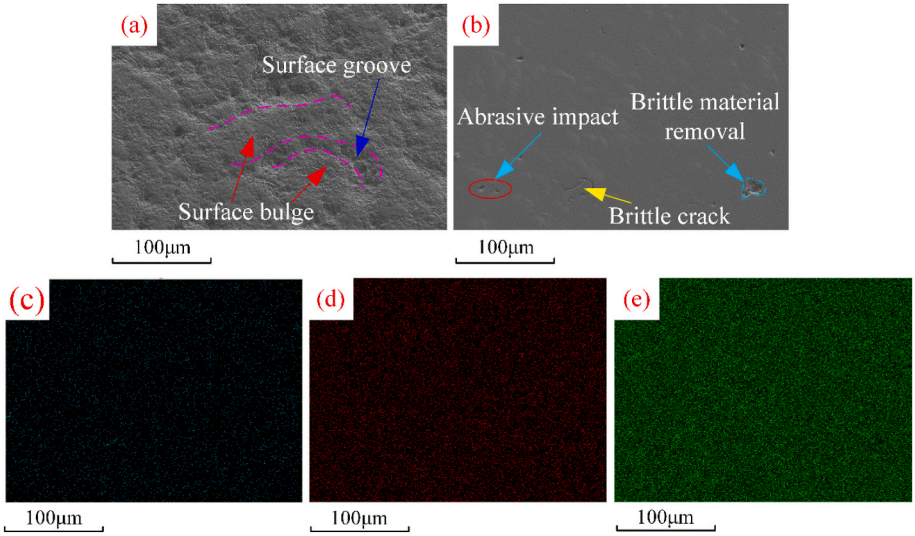

Fig. 3. The microscopic surface morphology and elements distribution of the ZrO_2 ceramic, (a) original surface, (b) processed surface, (c) C element, (d) O element, (e) Zr element.

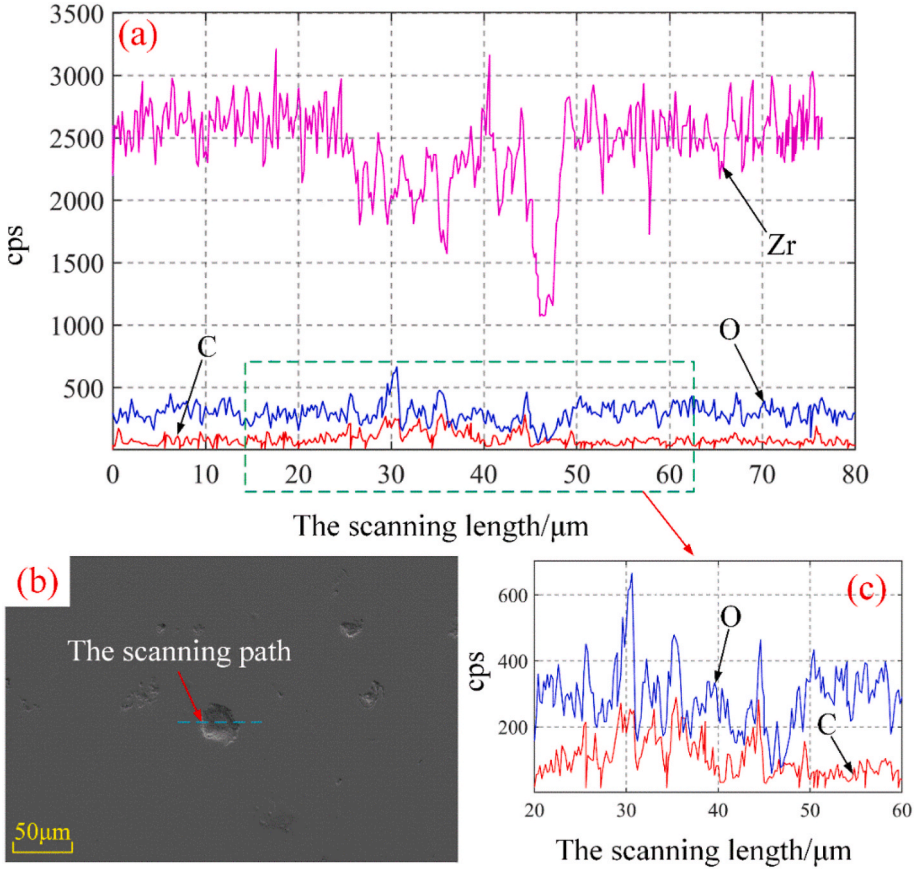

Fig. 4. The line scanning results of the ZrO_2 ceramic.

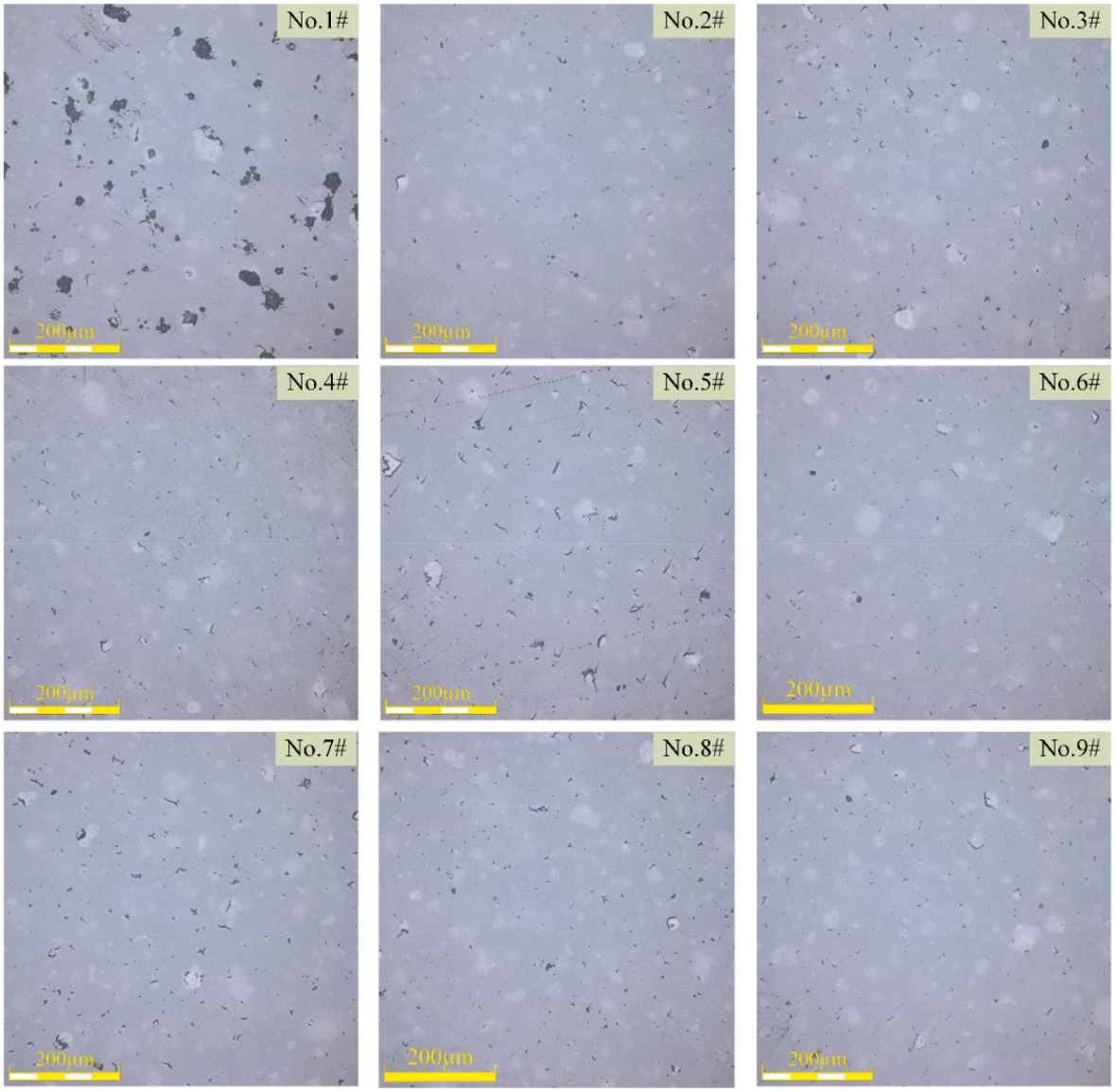

Fig. 5. The surface morphology of the ZrO_2 ceramic.

Table 4
The surface roughness of the ZrO_2 ceramic (μm).

No.	Spindle speed	Ultrasonic amplitude	Abrasive size	Surface roughness Ra			
				Value 1	Value 2	Value 3	Ave.
1#	2000 rpm	0 μm	0.05 μm	0.065	0.057	0.062	0.061
2#	2000 rpm	4 μm	0.5 μm	0.014	0.016	0.019	0.016
3#	2000 rpm	8 μm	1 μm	0.02	0.024	0.018	0.021
4#	5000 rpm	0 μm	0.5 μm	0.018	0.022	0.015	0.018
5#	5000 rpm	4 μm	1 μm	0.032	0.023	0.034	0.030
6#	5000 rpm	8 μm	0.05 μm	0.015	0.012	0.017	0.015
7#	8000 rpm	0 μm	1 μm	0.025	0.016	0.019	0.020
8#	8000 rpm	4 μm	0.05 μm	0.026	0.028	0.02	0.025
9#	8000 rpm	8 μm	0.5 μm	0.013	0.01	0.014	0.012

residual stress and micro-morphology, respectively. Due to the non-conductive nature of the ZrO_2 ceramic, it needs to be gold-sprayed prior to SEM analysis. During the residual stress measurement, the starting and ending angles of the X-ray scanning are 150° and 156°, respectively. The scanning time is 10min. The surface roughness is measured by the 3D laser confocal microscope (LEXT OLS41003D). The measuring instruments are shown in Fig. 2.

Table 1 shows the processing parameters during UVAP. The variables selected for the study are abrasive particle size, ultrasonic amplitude and spindle speed. The orthogonal experimental design is used to establish the UVAP experiments for the ZrO_2 ceramic, as shown in Table 2.

The ZrO_2 ceramic is characterized by difficult processing, superior wear resistance and high brittleness. Due to the inimitable physical property, the ZrO_2 ceramic is extensively applied in aerospace,

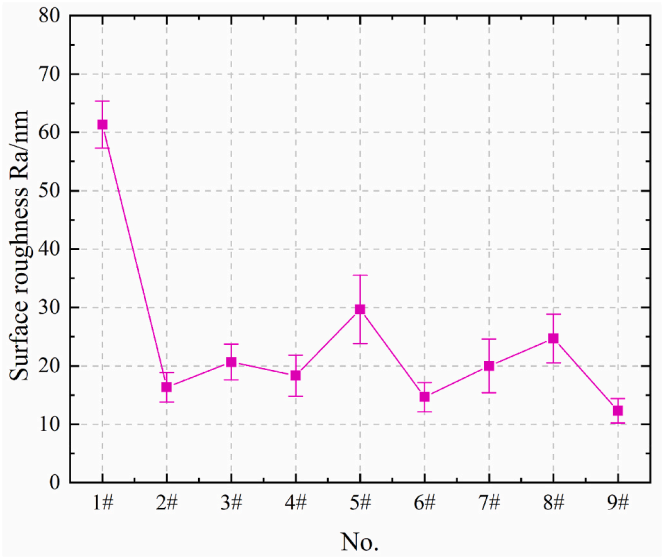

Fig. 6. The surface roughness of the ZrO_2 ceramic.

biomedical and other fields. With excellent cutting performance, the diamond is extensively employed in grinding and polishing procedures. Consequently, the diamond is adopted as the abrasive particle, which is homogeneously dispersed in the polishing slurry. The polyurethane material is used for the polishing tool. Table 3 lists the material properties of the ZrO_2, polyurethane and diamond.

3. Experimental results and analysis

3.1. Surface micro-morphology of the ZrO_2 ceramic

Fig. 3 denotes the microscopic surface morphology and elements distribution of the ZrO_2 ceramic. The original and processed surface morphology of the ZrO_2 are shown in Fig. 3(a) and **(b)**, respectively. Obviously, the original ZrO_2 is very poor with large areas of bulges and dents. The surface quality is greatly improved after the UVAP processing. The processed ZrO_2 surface is flattened to a higher degree than the original surface and there are no obvious bulges in the field of view. However, there are obvious cracks and defects in some areas where the abrasive particles impact microscopically.

In Fig. 3(c), the introduction of C element is observed. The distribution of C element is characterized by a relatively aggregation. The diamond abrasive particles act on the ZrO_2 surface with high-frequency impacts and scratches during the UVAP process. When the surface layer of the abrasive particle reaches failure limit, the residue of element C is formed on the ZrO_2 surface. Due to the effect of ultrasonic vibration, the intermittent cutting between the abrasive particles and the ZrO_2 ceramic is always maintained. Therefore, the distribution of C element is characterized by small areas of aggregation and is dispersed on the surface of ZrO_2 ceramic. Fig. 3(d) and **(e)** represent the elements of O and Zr on the ZrO_2 surface, respectively. Unlike the distribution characteristics of the C element, the distribution of the O element and Zr element is homogeneous and continuous with a dense nature.

To quantitatively analyze the C element, the line scanning for the ZrO_2 ceramic is required, as shown in Fig. 4. At the location of the abrasive impacting crater, there is a significant increase in the C element content, while the O element content shows unusual fluctuation. Outside the impacting zone, the change in element content tends to stabilize. The content change of C and O element tends to be synchronized within the impacting zone. The synergistic change of C and O element can be explained by the residual and oxidizing effect of C element from diamond on the surface of the ZrO_2 ceramic.

3.2. Surface roughness of ZrO_2 ceramic

Fig. 5 represents the surface morphology of the ZrO_2 ceramic. In Fig. 5, there are scratches caused by abrasive particle scratching and craters caused by abrasive particle impacting on the ZrO_2 surface. For different experiments, there are obvious differences in surface defects due to the effect of abrasive particle size and processing parameters. Therefore, a qualitative study on the machining quality of the ZrO_2 ceramic from the perspective of surface roughness is required.

The surface roughness of the ZrO_2 ceramic is shown in Table 4. The parameter Ra is selected to characterize the surface quality. In order to ensure the reliability of the experimental results, three parallel lines in the surface topography are selected to be analyzed and consider the average value (Ave.) as the final surface roughness. Fig. 6 represents the surface roughness result of the ZrO_2 ceramic. From Fig. 6, the surface quality of No.1#, No.5#, and No.8# experiments are poor. In contrast, the most excellent surface quality appears at the No.9# experiment. For both No.1# and No.8# experiments, the abrasive particle size is 0.05 μm. The abrasive particles of small size may be unevenly distributed on the ZrO_2 surface due to the agglomeration effect. In addition, the centrifugal force of the polishing slurry causes a large number of abrasive particles to be dispersed at the edge of the polishing tool, which ultimately leads to a degradation of the surface quality. The poor surface quality of No.5# experiment can be attributed to the large abrasive size and the spindle speed, which further exacerbates the inhomogeneous distribution of abrasive particles.

3.3. Residual stress of the ZrO_2 ceramic

Residual stress is an important indicator of the processing performance for the ZrO_2 ceramic. When the stress concentration exists on the workpiece surface, subsequent machining processes may result in cracks and damage to the material. The focus will be on the analysis of the relationship between processing parameters and residual stress. Fig. 7 shows the 2θ angle and FWHM results of the ZrO_2 ceramic. The final residual stress results are obtained by fitting as shown in Table 5 and Fig. 8. Meanwhile, the stress result of the original workpiece (No.0#) is selected for comparative analysis. The maximum value of surface stress occurs at No.9# experiment and the minimum value at No.7# experiment. The maximum value is about 6 times the minimum value. Therefore, the combinations of different processing parameters have a greater influence on the residual stress, and the selection of appropriate processing parameters can effectively improve the surface property and reduce the machining stress.

By analyzing the average and extreme value of the residual stress, it can be summarized that the spindle speed, ultrasonic amplitude and abrasive particle size have the following effect on the residual stress in descending order: abrasive particle size > spindle speed > ultrasonic amplitude. From a microscopic point of view, the generation of residual stress is directly associated with impacting and scratching process of abrasive particle. Although spindle speed and ultrasonic amplitude have a critical effect on the motion state of abrasive particle, the particle size determines changing difficulty of motion state. In addition, under the same working condition, the abrasive particle size is directly related to the material deformation and removal process of the ZrO_2 ceramic, which also has a greater influence on the processing stress.

From the abrasive particle size, the abrasive particle with the size of 0.5 μm has the greatest effect on the residual stress in Table 5. When the abrasive particle size is 0.05 μm, the abrasive particle is subjected to the drag force in the polishing slurry. In addition, the agglomeration

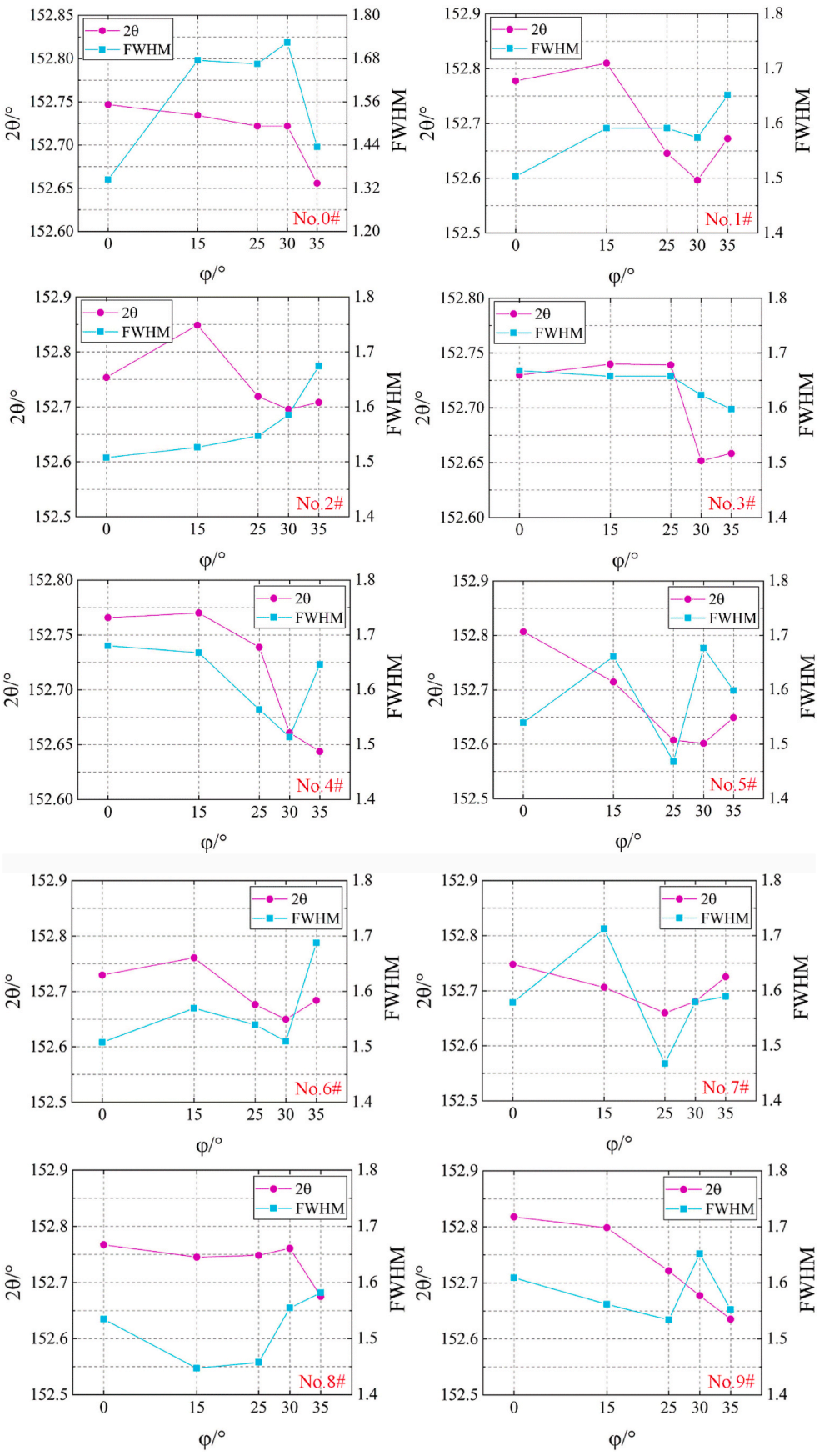

Fig. 7. The 2θ angle and FWHM results of the ZrO_2 ceramic.

Table 5
The residual stress results of the ZrO_2 ceramic (MPa).

No.	Spindle speed	Ultrasonic amplitude	Abrasive size	Residual stress
1#	2000 rpm	0 μm	0.05 μm	175
2#	2000 rpm	4 μm	0.5 μm	103
3#	2000 rpm	8 μm	1 μm	91
4#	5000 rpm	0 μm	0.5 μm	141
5#	5000 rpm	4 μm	1 μm	168
6#	5000 rpm	8 μm	0.05 μm	86
7#	8000 rpm	0 μm	1 μm	31
8#	8000 rpm	4 μm	0.05 μm	65
9#	8000 rpm	8 μm	0.5 μm	195
Ave. at level 1	123	115.67	108.67	–
Ave. at level 2	131.67	112	146.33	–
Ave. at level 3	97	124	96.67	–
Extreme deviation	34.67	12	49.66	–

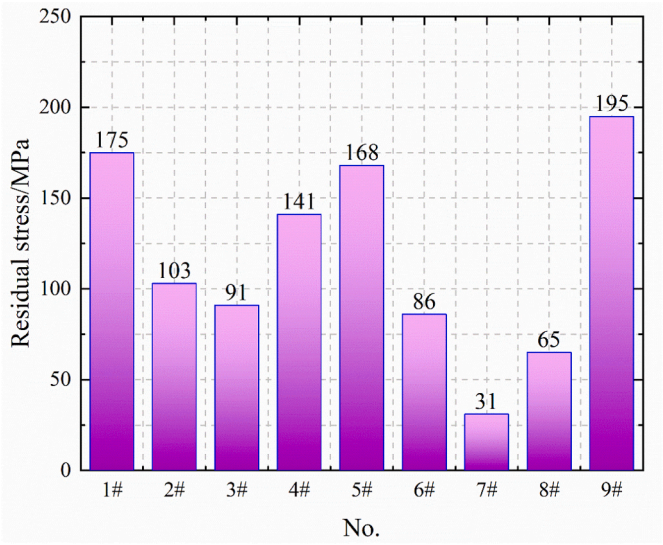

Fig. 8. The residual stress results of the ZrO_2 ceramic.

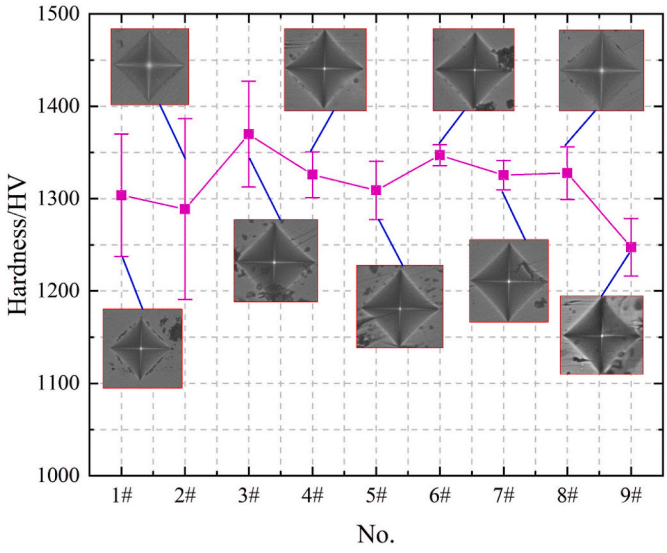

Fig. 9. Average surface hardness of the ZrO_2.

phenomenon that occurs in the abrasive particles themselves also leads to a restricted state of motion. The number of abrasive particles acting on the ZrO_2 is reduced in the same machining area when the abrasive particle size is 1 μm. During the entire machining process, the number of abrasive particles acting at the same area is reduced. This leads to a reduction of the stress accumulation effect, which in turn weakens the effect on the residual stress.

3.4. Surface hardness of the ZrO_2 ceramic

Fig. 9 presents the average surface hardness of the ZrO_2 ceramic. The maximum value of surface hardness appeared at No.3# experiment with 1369.83HV. The minimum value appeared at No.9# experiment with 1247.33HV. Combined with the processing parameters, the ultrasonic amplitude and abrasive particle size are level 3 in the No.3# experiment. This may be due to the fact that the larger ultrasonic amplitude and abrasive particle size affect the kinetic energy and impacting velocity of the abrasive particle. This resulted in the introduction of an amorphous hardened layer on the ZrO_2 ceramic surface. The material grains from the amorphous layer are tightly packed and uniformly refined. In comparison with the ZrO_2 substrate, the hardness of amorphous layer is significantly higher.

For No.9# experiment, the spindle speed and ultrasonic amplitude correspond to level 3. The higher the spindle speed, the greater material removal is created in the same processing time. As the amorphous layer structure is removed, the softer substrate of the ZrO_2 ceramic is more susceptible to exposure. Although larger ultrasonic amplitude leads to a strong abrasive particle impact and surface hardening effect, the hardness strengthening is limited compared with the hardness from exposed substrate structure. As a result, the surface hardness still tends to decrease on the macroscopic scale.

Table 6 lists the surface hardness of ZrO_2. From the extreme deviation of the average hardness, the influence trend of each factor on the surface hardness in descending order is: abrasive particle size > spindle speed > ultrasonic amplitude. This is similar to the result of the stress analysis, and the effect of abrasive particle size on surface hardness is also the most significant, with ultrasonic amplitude contributing the least. Combined with the previous analysis, the abrasive particle size has a direct effect on the introduction of the amorphous layer and material removal. Even though the ultrasonic amplitude and spindle speed can also play a role in changing the surface hardness, they have a weaker effect on the surface hardness than the abrasive particle size. It is worth noting that the standard deviation is generally larger in the experiments with spindle speed of level 1 and level 2 compared to level 3. This may be due to the fact that the cutting number and contact time of the abrasive particles per unit area on the ZrO_2 ceramic surface is reduced when the spindle speed is low, resulting in uneven material removal. The amorphous layer structure of the ZrO_2 ceramic alternates with the substrate material, resulting in a large standard deviation of the surface hardness.

3.5. Surface scratching performance of the ZrO_2 ceramic

The scratching experiment is conducted by a diamond indenter on the ZrO_2 ceramic surface, and the scratching coefficient can reflect the material property as well as the surface quality from the microscopic point of view. The hardness strengthening and material removal behaviors exist on the ZrO_2 ceramic after UVAP processing. During the scratching process, the material accumulation and extrusion occur near the diamond indenter, which is directly reflected in the scratching coefficient curve. Fig. 10 shows the scratching process on the ZrO_2 ceramic. The starting point is located on the original surface of the ZrO_2 to emphasize the scratching effect. Meanwhile, the comparative experiment is conducted on the unprocessed ZrO_2 ceramic.

The scratching coefficient of the ZrO_2 ceramic with loading force is shown in Fig. 11. From Fig. 11, the scratching coefficient appears to

Table 6
The surface hardness of ZrO_2 (HV).

No.	Spindle speed	Ultrasonic amplitude	Abrasive size	Hardness			
				Value 1	Value 2	Value 3	Ave.
1#	2000 rpm	0 μm	0.05 μm	1380.3	1262.2	1268.7	1303.73
2#	2000 rpm	4 μm	0.5 μm	1374.1	1310	1181.9	1288.67
3#	2000 rpm	8 μm	1 μm	1433.7	1323.7	1352.1	1369.83
4#	5000 rpm	0 μm	0.5 μm	1322.7	1352.2	1302.9	1325.93
5#	5000 rpm	4 μm	1 μm	1343.8	1281.9	1301.1	1308.93
6#	5000 rpm	8 μm	0.05 μm	1336.7	1359.3	1345	1347.00
7#	8000 rpm	0 μm	1 μm	1316.7	1315.8	1343.8	1325.43
8#	8000 rpm	4 μm	0.05 μm	1322.7	1302	1358.3	1327.67
9#	8000 rpm	8 μm	0.5 μm	1211.8	1269.9	1260.3	1247.33
Ave. at level 1	1320.74	1318.37	1326.13	–			
Ave. at level 2	1327.29	1308.42	1287.31	–			
Ave. at level 3	1300.14	1321.39	1334.73	–			
Extreme deviation	27.15	12.97	47.42	–			

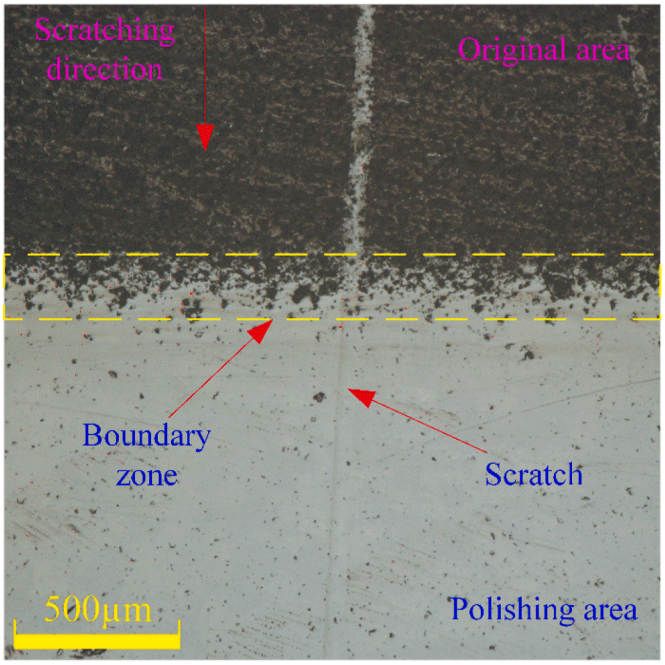

Fig. 10. The scratching process on the ZrO_2 ceramic.

increase with the increase of loading force. There is a significant difference between the original surface and processed surface for the scratching coefficient of the ZrO_2 ceramic, and the surface quality directly affects the trajectory of the diamond indenter and scratching coefficient results. The scratching coefficient of the processed surface is more stable compared with the original surface. The smaller fluctuation range of the scratching coefficient indicates that the surface quality of the polished area is better. In this study, the average and extreme deviation of the scratching coefficient are selected to quantitatively compare the scratching property and surface quality. The average of the scratching coefficient reflects the variation in the surface property of the ZrO_2 ceramic, while the standard deviation reflects the stability and consistency of the material property within the scratching path.

Fig. 12 presents the average and standard deviation of the scratching coefficient. From the experimental results, the maximum value of the average scratching coefficient is 0.1081 in the No.9# experiment, and the minimum value is 0.0794 in the No.5# experiment. In general, there is no significant fluctuation in the variation of the average scratching coefficient. It indicates that the change in the surface property of the ZrO_2 ceramic has no substantial effect on the average scratching coefficient within the range of the selected processing parameters. In terms of the standard deviation, the maximum value is 0.0211 in control experiment No.0#, and the minimum value is 0.0057 in No.7# experiment. The standard deviation results of the scratching coefficient for other experiments are maintained at a low level compared to the No.0#. This indicates that the stability of surface property and surface quality for the polished ZrO_2 ceramic are significantly improved compared with the unprocessed ZrO_2 ceramic. From the perspective of ultrasonic vibration, the standard deviation of the scratching coefficient is the lowest at an amplitude of 0 μm. This indicates that the introduction of ultrasonic vibration brings great uncertainty to the variation of surface property, and the variability of surface property increases in different processing regions.

Table 7 and Table 8 show the results of the average and standard deviation of the surface scratching coefficient. In terms of the average scratching coefficient, the influence trend of each processing parameter on the scratching performance of the ZrO_2 ceramic surface in descending order is as follows: abrasive particle size > spindle speed > ultrasonic amplitude. Combined with the previous analysis, this result is the same as that of surface hardness and residual stress. The influence of ultrasonic amplitude is still weaker than that of abrasive particle size and spindle speed. In terms of the standard deviation, the influence of each machining parameter on the scratching performance in descending order is as follows: spindle speed > ultrasonic amplitude > abrasive particle size. The ultrasonic amplitude and spindle speed have a greater influence on the stability of the surface property of the ZrO_2 ceramic. Therefore, the ultrasonic amplitude and spindle speed can be considered to improve the stability and consistency of the surface property for the ZrO_2 ceramic during UVAP processing.

4. Conclusions

This paper investigates the surface integrity of ZrO_2 ceramic during UVAP processing. The main findings may include:

(1) The craters caused by diamond impacting can be clearly seen on the processed surface of ZrO_2, and obvious C-element aggregation in the impacting crater is found. The generation of residual stress has a direct relationship with the abrasive particle impacting and scratching. Although the spindle speed and ultrasonic amplitude have a direct effect on the motion state of abrasive particle, the particle size determines the changing difficulty of the motion state. In addition, the abrasive particle size is directly related to

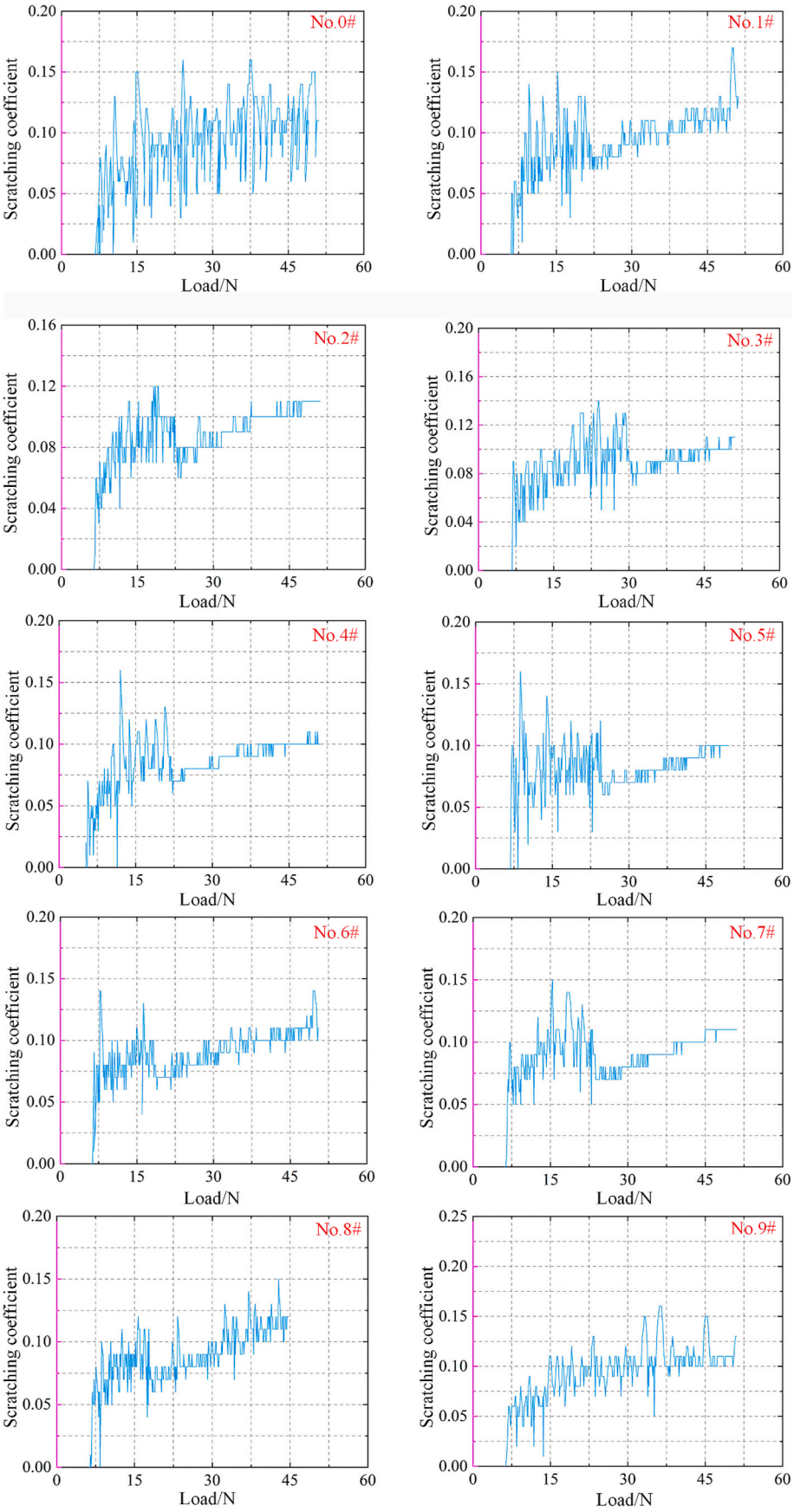

Fig. 11. The scratching coefficient of the ZrO_2 ceramic with loading force.

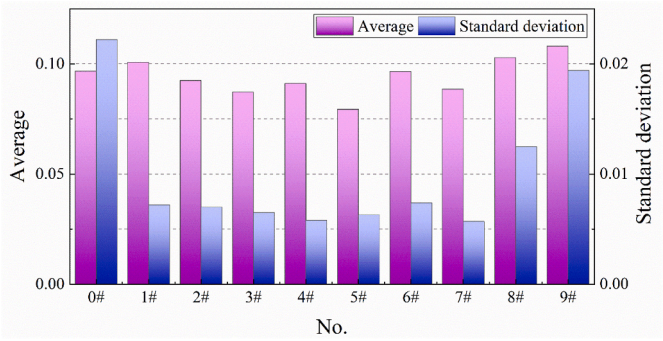

Fig. 12. Average and standard deviation of the surface scratching coefficient.

Table 7
The average of the scratching coefficient.

No.	Spindle speed	Ultrasonic amplitude	Abrasive size	Ave.
1#	2000 rpm	0 μm	0.05 μm	0.1007
2#	2000 rpm	4 μm	0.5 μm	0.0925
3#	2000 rpm	8 μm	1 μm	0.0872
4#	5000 rpm	0 μm	0.5 μm	0.0911
5#	5000 rpm	4 μm	1 μm	0.0794
6#	5000 rpm	8 μm	0.05 μm	0.0966
7#	8000 rpm	0 μm	1 μm	0.0885
8#	8000 rpm	4 μm	0.05 μm	0.1028
9#	8000 rpm	8 μm	0.5 μm	0.1081
Ave. at level 1	0.0935	0.0934	0.1000	–
Ave. at level 2	0.0890	0.0916	0.0972	–
Ave. at level 3	0.0998	0.0973	0.0850	–
Extreme deviation	0.0108	0.0057	0.015	–

Table 8
The standard deviation of the scratching coefficient.

No.	Spindle speed	Ultrasonic amplitude	Abrasive size	Standard deviation
1#	2000 rpm	0 μm	0.05 μm	0.0071
2#	2000 rpm	4 μm	0.5 μm	0.0069
3#	2000 rpm	8 μm	1 μm	0.0065
4#	5000 rpm	0 μm	0.5 μm	0.0058
5#	5000 rpm	4 μm	1 μm	0.0062
6#	5000 rpm	8 μm	0.05 μm	0.0073
7#	8000 rpm	0 μm	1 μm	0.0057
8#	8000 rpm	4 μm	0.05 μm	0.0125
9#	8000 rpm	8 μm	0.5 μm	0.0192
Ave. at level 1	0.0068	0.0062	0.0090	–
Ave. at level 2	0.0064	0.0085	0.0106	–
Ave. at level 3	0.0125	0.0110	0.0061	–
Extreme deviation	0.0061	0.0048	0.0045	–

the material deformation and removal of the ZrO_2 ceramic under the same working condition, which also has a greater impact on the processing stress.

(2) The ultrasonic amplitude and abrasive particle size affect the impacting velocity and kinetic energy. This leads to the introduction of an amorphous hardened layer on the original surface of the ZrO_2 ceramic. The softer substrate is exposed as the surface amorphous layer is removed. Although the larger ultrasonic amplitude leads to a strong abrasive particle impact and surface hardening effect, the hardness strengthening is limited compared with the hardness of exposed substrate structure. As a result, the surface hardness still shows a decreasing trend on a macroscopic scale.

(3) Within the selected range of processing parameters, the change in the surface property of the ZrO_2 ceramic has no substantial effect on the average of the scratching coefficient. Compared with the control experiment No.0#, the standard deviation results of the scratching coefficient for other experiments remain at a low level. The stability of surface property for the polished ZrO_2 ceramic is significantly improved compared to the unprocessed ZrO_2 ceramic. The introduction of ultrasonic vibration brings great uncertainty to the change of surface property for the ZrO_2 ceramic, and the variability of surface property increases in different processing regions.

Declaration of competing interest

The authors declare that they have no known competing financial interests or personal relationships that could have appeared to influence the work reported in this paper.

Acknowledgments

This work was funded from the Major State Basic Research Development Program of China [Grant No. 2017YFA07]; Fundamental Research Funds for the Central Universities [Grant No.2103001].

References

[1] L. Chao, Z. Junjie, L. Xiangfeng, et al., Facile laser-based process of superwetting zirconia ceramic with adjustable adhesion for self-cleaning and lossless droplet transfer, Appl. Surf. Sci. 638 (2023), 158069, https://doi.org/10.1016/j.apsusc.2023.158069.
[2] W. Li, Y. Hang, H. Zongdong, et al., Investigating the effect of solid loading on microstructure, mechanical properties, and translucency of highly translucent zirconia ceramics prepared via stereolithography-based additive manufacturing, J. Mech. Behav. Biomed. Mater. 144 (2023), 105952, https://doi.org/10.1016/j.jmbbm.2023.105952.
[3] Y. Xuefeng, Research on Optimization of Machining Parameters for Milling Zirconia Ceramics with PCD Tools [D], North China University of Science and Technology, Tangshan, 2021, https://doi.org/10.27108/d.cnki.ghelu.2021.000058.
[4] Q. He, J. Jiang, X. Yang, et al., Additive manufacturing of dense zirconia ceramics by fused deposition modeling via screw extrusion, J. Eur. Ceram. Soc. 41 (1) (2020) 1033–1040, https://doi.org/10.1016/j.jeurceramsoc.2020.09.018.
[5] Y. Min, L. Changhe, S. Zafar, et al., Semiempirical heat flux model of hard-brittle bone material in ductile micro grinding, J. Manuf. Process. 71 (2021) 501–514, https://doi.org/10.1016/j.jmapro.2021.09.053.
[6] L. Mingzheng, L. Changhe, Z. Yanbin, et al., Analysis of grain tribology and improved grinding temperature model based on discrete heat source, Tribol. Int. 180 (2023), 108196, https://doi.org/10.1016/j.triboint.2022.108196.
[7] F. Cheng, L. Kaixuan, C. Yigang, et al., A new modelling method of material removal profile for electrorheological polishing with a mini annular integrated electrode, J. Mater. Process. Technol. 305 (2022), 117589, https://doi.org/10.1016/J.JMATPROTEC.2022.117589.
[8] Z. Lei, D. Chen, H. Yanjun, et al., Investigation into a novel pulsating cavitation air jet polishing method for Ti-6Al-4V alloy, Tribol. Int. 175 (2022), 107837, https://doi.org/10.1016/j.triboint.2022.107837.
[9] W. Zhao, M. Zhelun, C. Tao, et al., Experimental investigation into the effect of process parameters on the Inconel 718 surface integrity for abrasive waterjet peening, Surf. Coating. Technol. 454 (2023), 129186, https://doi.org/10.1016/j.surfcoat.2022.129186.
[10] X. Wenhu, S. Chong, Z. Min, Effects of ultrasonic vibration on sapphire polishing investigated by molecular dynamics, Tribol. Int. 176 (2022), 107911, https://doi.org/10.1016/J.TRIBOINT.2022.107911.
[11] D. Hongguang, Z. Min, X. Wenhu, Effects of different dispersants on chemical reaction and material removal in ultrasonic assisted chemical mechanical polishing of sapphire, ECS J. Solid State Sci. Technol. 11 (3) (2022), 033007, https://doi.org/10.1149/2162-8777/AC5A6D.
[12] N. Kobayashi, Y. Wu, M. Nomura, et al., Precision treatment of silicon wafer edge utilizing ultrasonically assisted polishing technique, J. Mater. Process. Technol. 201 (2008) 531–535, https://doi.org/10.1016/j.jmatprotec.2007.11.220.
[13] H. Suzuki, T. Moriwaki, T. Okino, et al., Development of ultrasonic vibration assisted polishing machine for micro aspheric die and mold, CIRP Ann. - Manuf. Technol. 55 (1) (2006) 385–388, https://doi.org/10.1016/S0007-8506(07)60441-7.
[14] H. Suzuki, S. Hamada, T. Okino, et al., Ultraprecision finishing of micro-aspheric surface by ultrasonic two-axis vibration assisted polishing, CIRP Ann.-Manuf. Technol. 59 (1) (2010) 347–350, https://doi.org/10.1016/j.cirp.2010.03.117.

[15] S. Zhiyuan, Research on Ultrasonic Vibration Polishing Technology for Microstructured Optically Functional Surfaces of Hard and Brittle Materials [D], Harbin Institute of Technology, Harbin, 2015.
[16] W. Changhao, Research on Vibration-Assisted Polishing Process for Superhard Microstructured Optical Surfaces [D], Harbin Institute of Technology, Harbin, 2013.
[17] F. Cheng, Research on Face Accuracy Control for Deterministic Polishing of Optical Surfaces [D], Jilin University, Jilin, 2014.
[18] W. Guilian, W. Yiqiang, X. Zhixing, Modeling and analysis of the material removal depth for stone polishing, J. Mater. Process. Technol. 209 (5) (2008) 2453–2463, https://doi.org/10.1016/j.jmatprotec.2008.05.041.
[19] L. Jinxin, Mechanism and Experimental Study of Ultrasonic Vibration-Assisted Polishing of BK7 Optical Glass [D], Northeastern University, Shenyang, 2020.
[20] S. Dong, Ultrasound-assisted Grinding and Chemical-Mechanical Polishing of Single-Crystal SiC Wafers [D], Jilin University, Jilin, 2019.
[21] W. Zhihui, Research on the Removal Mechanism of Single Crystal Silicon Material by Ultrasonic Vibration-Assisted Polishing [D], Northeastern University, Shenyang, 2019.
[22] S. Chong, Molecular Dynamics Study of the Effect of Ultrasonic Vibration on CMP of Sapphire [D], Nanchang University, Nanchang, 2022.